Geomechanics and Engineering, *Vol. 27, No. 6 (2021) 583-594*
https://doi.org/10.12989/gae.2021.27.6.583

Research on sealing ability of granular bentonite material after 10.5 years of engineered barrier experiment

Hongyang Ni[1,2a], Jiangfeng Liu*[1,3], Hai Pu[1b], Guimin Zhang[1c], Xu Chen[1d] and Frédéric Skoczylas[2e]

[1]*State Key Laboratory for GeoMechanics and Deep Underground Engineering, and School of Mechanics and Civil Engineering, China University of Mining & Technology, Xuzhou 221116, China*
[2]*Laboratoire de Méchanique de Lille (LML), and École Centrale de Lille, BP 48, F-59651 Villeneuve d'Ascq Cedex, France*
[3]*CAEA Innovation Center on Geological Disposal of High Level Radioactive Waste, Beijing Research Institute of Uranium Geology, China*

(*Received July 28, 2020, Revised October 22, 2021, Accepted November 10, 2021*)

Abstract. The gas permeability behavior of unsaturated bentonite-based materials is of major importance for ensuring effective sealing of high-level radwaste repositories. This study investigated this by taking a sample of Granular Bentonite Material (GBM) at the end of the Engineered Barrier Emplacement (EB) experiment in the Opalinus Clay, placing it under different humidity conditions until it achieved equilibration, and testing the change in the gas permeability under loading and unloading. Environmental humidity is shown to have a significant effect on the water content, saturation, porosity and dry density of GBM and to affect its gas permeability. Higher sensitivity to confining pressure is exhibited by samples equilibrated at higher relative humidity (RH). It should be noted that for the sample at RH=98%, when the confining pressure is raised from 1 MPa to 6 MPa, gas permeability can be reduced from 10^{-16} m^2 to 10^{-19} m^2, which is close to the requirements of gas tightness. Due to higher water content and easier compressibility, samples equilibrated under higher RH show greater irreversibility during the loading and unloading process. The effective gas permeability of highly saturated samples can be increased by 2–3 orders of magnitude after 105°C drying. In addition, cracks possibly occurred during the dehydration and drying process will become the main channel for gas migration, which will greatly affect the sealing performance of GBM.

Keywords: effective gas permeability; granular bentonite material; irreversible change; microstructure

1. Introduction

Deep geological disposal is an internationally accepted method of disposing of nuclear waste (Davy *et al*. 2008). After high-level radioactive waste is solidified and canned, it is buried 500-1000 m underground and sealed by buffer/backfill material (bentonite) (Dueck 2008, Pusch 1979). Groundwater seepage causes the bentonite to swell as it absorbs water, filling the gap between bentonite blocks and between the bentonite and the surrounding rock, thus achieving a sealing function. During the long-term evolution of repositories, CO_2, CH_4, N_2, and other gases will be generated due to the corrosion of storage containers, the decomposition of microorganisms, and the radiolysis of water (Ortiz *et al*. 2002). The accumulation of these gases will affect the stability and safety of the entire repository (Galle 2000). The characteristics of gas migration have therefore become a key scientific issue in deep geological disposal research.

Due to their water-retention and swelling behavior, pure bentonite, bentonite–sand mixtures, and bentonite with clay rock offer good sealing performance at low gas pressure (<2.6 MPa) under saturation conditions (Czaikowski *et al*. 2014, Zhang and Krohn 2019). This is because the gas pressure has little effect on the saturation of the sample at low pressure. However, a gas pressure greater than 6 MPa will have a marked effect on the saturation, reducing the sealing performance of the bentonite (Liu *et al*. 2017). The characteristics of gas migration are significantly influenced by water content (saturation) and dry density (Wei *et al*. 2019). This has been demonstrated by the Full-Scale Engineered Barriers Experiment (FEBEX) in-situ test, which is a full-scale experiment performed at the Grimsel Test Site (Switzerland) under natural conditions to reproduce the Engineered Barrier System of an underground repository for high-level radioactive waste. When the bentonite on the outside of the canister (simulated by a heater) was hydrated over 18 years, associated research shows that gas permeability decreases with an increase in water content and dry density. The permeability of the sample is related to its position in the barrier. Since groundwater flows from the outside to the inside of the barrier, the side closest to the surrounding granite has high water content and low dry density, its saturation is higher than deeper within the barrier, and it thus has better sealing ability (Carbonell *et al.* 2019).

When the dry density is low, both mechanical and capillary effects have important influences on the gas

*Corresponding author, Professor
E-mail: jeafliu@cumt.edu.cn
[a]Ph.D. Student
[b]Ph.D.
[c]Ph.D.
[d]Ph.D.
[e]Ph.D.

ISSN: 2005-307X (Print), 2092-6219 (Online)

migration characteristics, but with an increase in dry density, the capillary effect becomes the main factor. The gas migration characteristics are closely related to the swelling pressure (Sun 2018, Angin *et al*. 2018). Under a rigid boundary condition, the gas breakthrough pressure is greater than the swelling pressure but is smaller than the gas entry pressure of a water retention test, and with an increase in dry density, it will come closer to the gas entry pressure (Xu *et al*. 2017). The increase in dry density changes the porosity of the sample and thus changes the gas flow path, as the gas will preferentially flow through larger interconnected pores. It should be pointed out that a smaller particle size often leads to lower permeability (Gutierrez-Rodrigo *et al*. 2014).

External environmental conditions also have significant effects on the gas permeability of bentonite (Niu *et al.* 2019). There is strong coupling between stress, gas pressure and flow in bentonite: a large-scale gas injection test (Lasgit) performed at the Aspo Hard Rock Laboratory shows pathway dilation to be the primary mechanism governing gas migration (Cuss *et al.* 2011, Harrington *et al.* 2017). Gas migration is related to the development of preferential paths along existing or pressure-dependent discontinuities (Olivella and Alonso, 2008), and this is influenced by the stress–strain boundary conditions, as these affect the swelling properties (Sun *et al.* 2017, Tang *et al*. 2019). When the gas pressure approaches the sum of the porewater pressure and the swelling pressure, gas entry is seen to occur (Graham *et al*. 2012). An increase in confining pressure will lead to an irreversible increase in dry density and will therefore reduce the permeability. It should be pointed out that, for water-saturated samples, when the confining pressure is greater than 4 MPa, there is no gas flow observed in the sample, while for dry samples, even if the confining pressure reaches 9 MPa, gas can continue to flow (Carbonell *et al.* 2019). Gas permeability is more sensitive to confining pressure than to gas pressure, and when the relative humidity (RH) of the environment reaches 98%, although the sample is not saturated, it can still play a sealing role when a confining pressure of 7–8 MPa is applied (Liu *et al.* 2018).

With the aim of demonstrating that good sealing performance can be achieved by automated production of Granular Bentonite Material (GBM) and its emplacement in the upper part of a clay barrier, ENRESA (Empresa Nacional de Residuos Radioactivos SA) initiated the Engineered Barrier Emplacement Experiment (EB experiment), a full-scale test in the Opalinus Clay formation, in October 2000 (García-Siñeriz *et al.* 2008, Mayor *et al*. 2005, Villar 2012). The experimental layout is shown in Fig. 1. After 10.5 years of hydration, the experiment was dismantled and samples from it were subjected to laboratory analysis. The results show that the GBM became perfectly homogeneous, with a high water content, and that it had an optimal sealing capacity (Garcia-Sineriz *et al*. 2015, Liu *et al.* 2016). However, in the repository environment, the bentonite would also be subjected to drying process due to gas migration and the heat from radioactive waste (Seiphoori *et al.* 2014). Therefore work remains to be carried out to clarify the permeability of GBM in the dehydration process. This study sets out to remedy this deficiency.

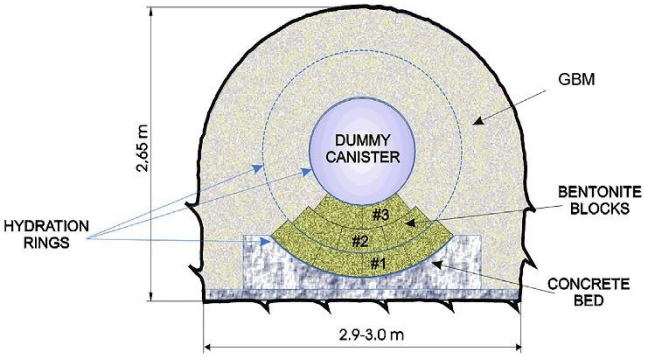

Fig. 1 Layout of Engineered Barrier Emplacement Experiment (García-Siñeriz *et al*. 2008)

2. Material preparation and experimental methodology

2.1 Materials and sample preparation

The material tested was a sample of the GBM from the upper right part in Fig. 1, more detailed information on its location can be found in (Liu *et al.* 2016). It was prepared from FEBEX bentonite with a specific gravity of 2.70±0.04 g/cm^3. The specific physicochemical properties, composition and particle size distribution of GBM after the EB experiment can be found in (Villar 2012).

The GBM was wrapped in plastic film immediately after being taken from the site, was vacuum packaged for transport to the laboratory, and was further prepared by molding in a round mold. The sample height was 25 ± 1 mm, and the diameter was 37 ± 0.5 mm. The initial characteristics are shown in Table 1, where ρ_{bulk} is bulk density, ρ_d is dry density, ω is water content, φ is porosity, and S_r is saturation. It can be seen that after 10.5 years of hydration, expansion due to water absorption had caused a reduction in the dry density of the GBM, while both water content and porosity increase, and saturation is approaching 1, which indicates that the samples had achieved a quasi-saturated state.

2.2 Experimental method

This test was designed to study the sealing performance of unsaturated GBM in the upper right part in Fig. 1. Due to losses during drilling and sample preparation, the final four cylindrical samples successfully obtained were named GBM-1, GBM-2, GBM-3, and GBM-4, they were placed in relative humidity conditions of 11%, 75%, 85%, and 98%, respectively, and under free swelling condition, to test their water retention characteristics. As there is no way to guarantee identical initial characteristics for the samples available from the field site, they were placed at different humidity levels depending on the initial saturation. The specified relative humidity was achieved by vapor equilibrium technique, i.e. by configuring different saturated salt solutions to create different relative humidity. The four saturated salt solutions and the corresponding relative humidity are shown in Table 2.

Table 1 Characteristics of the GBM samples in their initial state for this study (Liu *et al.* 2016)

Parameters	ρ_{bulk}(g/cm^3)	ρ_d(g/cm^3)	ω(%)	φ	S_r
GBM-1	1.65	1.22	35.72	0.55	0.8
GBM-2	1.65	1.22	35.72	0.5	0.8
GBM-3	1.74	1.33	30.97	0.51	0.81
GBM-4	1.65	1.14	44.88	0.58	0.89

Table 2 Different saturated salt solutions and the corresponding relative humidity for samples

Saturated salt solutions	LiCl	NaCl	KCl	K_2SO_4
RH (%)	11	75	85	98
Samples	GBM-2	GBM-2	GBM-3	GBM-4

At the same time, four small specimens with the same characteristics were also placed in the different relative humidity environments, respectively, for electron microscopic analysis. It was performed by environmental scanning electron microscope (ESEM) FEI Quanta^{TM} 250. It is capable of maintaining desired environmental conditions across a range of relative humidity during the detection of the sample structure. Sample desiccation and coating are not required, and, as a result, sample disturbance is minimized and the micrographs are more representative (Lin and Cerato 2014, Montes-H 2005, Sun *et al*. 2019). With a magnification of 1000 and a resolution of 3.45 μm, pores and cracks with size larger than 3.45 μm can be observed.

A steady state was judged to have been achieved when the mass change of the unsaturated GBM was less than 1‰ in two consecutive measurements. Gas permeability measurements were then carried out.

Gas permeability was measured throughout a loading–unloading sequence to determine whether there was irreversible change in the sealing performance of the material; the loading path applied was 1–1.5–3–4.5–6–4.5–3–1.5–1 MPa. On the basis that swelling pressure can reach 6-7 MPa when the mixture approaches saturation (Gatabin, 2005) while the material studied in this paper is in an unsaturated state, the maximum confining pressure was set at 6 MPa. Previous research results show that the steady-state method has higher accuracy for measuring the permeability of porous media where that permeability is greater than 10^{-19} m^2. When the permeability is less than this value, accurate measurement can be obtained by extending the measurement time (Billiotte *et al.* 2008). Therefore the steady-state method was used in this experiment.

As shown in Fig. 2, during the measurement, the sample is placed inside the cylinder. The valve between the gas tank and the buffer reservoir is opened, and gas is injected into the buffer reservoir to reach a certain pressure P_1. The gas pressure can be read from the pressure gauge between the buffer reservoir and the gas storage unit. After that, the valve is closed, and the valve connecting the reservoir buffer and the inlet end of the sample is opened to start gas

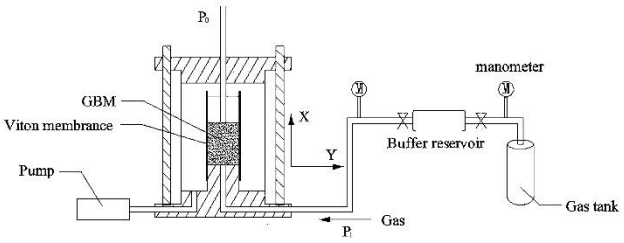

Fig. 2 Schematic diagram of the steady state method

injection into the sample. The pressure change during this process can be read from the pressure gauge. After time interval Δt, the gas pressure becomes P_1-ΔP, and the average pressure in the reservoir buffer is

$$P_{mean} = \frac{P_1 + P_1 - \Delta P}{2} = P_1 - \frac{\Delta P}{2} \tag{1}$$

Based on Darcy's law, the average flow rate during this time period is

$$Q_{mean} = -k \frac{A}{\mu} \frac{\partial P}{\partial x} \tag{2}$$

where k is the permeability, A is the cross-sectional area of the sample, and μ is the dynamic viscosity

On the basis of the principle of mass conservation (which dictates that the mass of gas flowing out of the buffer reservoir is equal to the mass of gas passing through the sample)

$$\Delta P V_0 = P_{mean} Q_{mean} \Delta t \tag{3}$$

which is

$$Q_{mean} = \frac{V_0 \Delta P}{P_{mean} \Delta t} \tag{4}$$

where V_0 is the volume of the buffer reservoir.

According to (Dana and Skoczylas 1999), the distribution of the compressible gas pressure in the sample is a function of the coordinate x and the time interval t

$$P(x,t) = \sqrt{P(0,t)^2 \left(1 - \frac{x}{h}\right) + P(h,t)^2 \frac{x}{h}} \tag{5}$$

where h is the height of the sample, $P(0,t)=P_{mean}$, $P(h,t)=P_0$, and P_0 is atmospheric pressure. The formula for calculating the effective gas permeability can be obtained through consideration of Eqs. (2)-(5).

$$k = \frac{\mu V_0 \Delta P}{A \Delta t} \frac{2h}{P_{mean}^2 - P_0^2} \tag{6}$$

3. Results and discussion

3.1 Characteristics of the sample after equilibration under different RH conditions

Figs. 3(a)-3(d) show the saturation, water content,

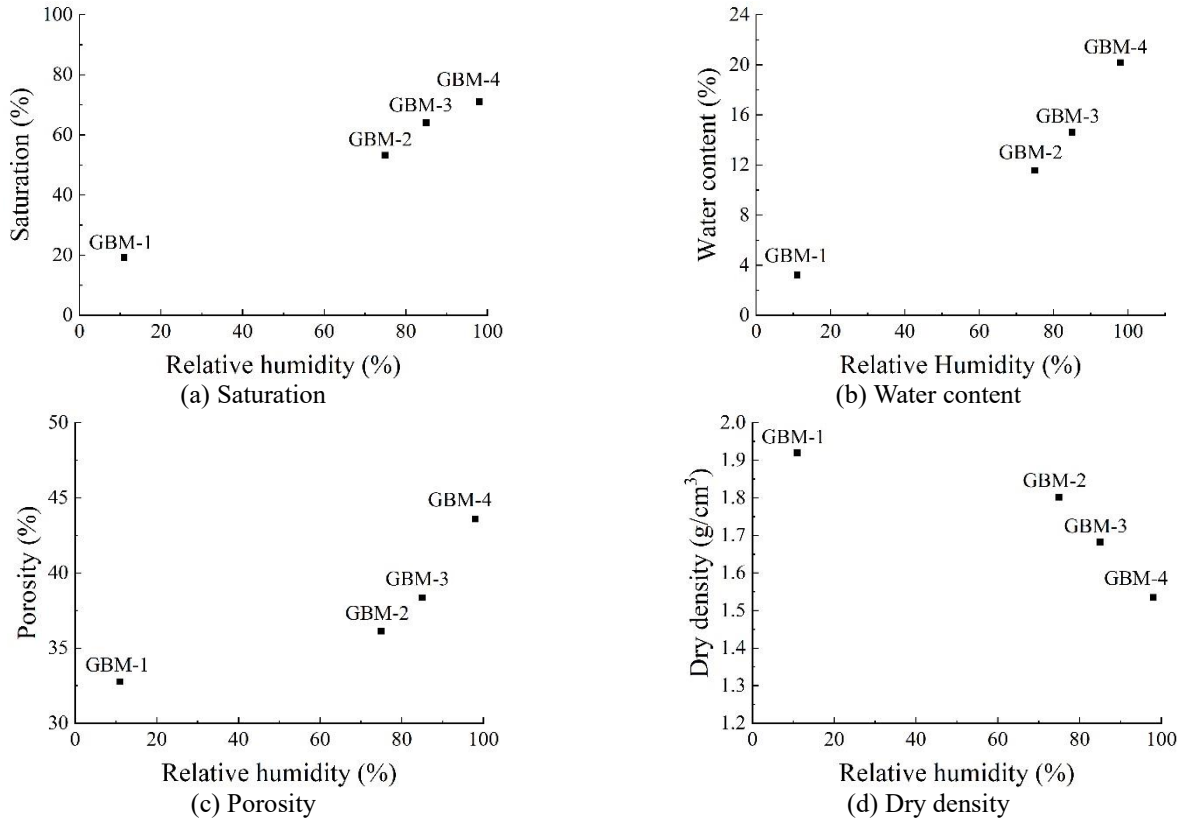

Fig. 3 Saturation, Water content, Porosity and Dry density after equilibration under different RH conditions

porosity, and dry density changes of the samples after equilibration under different humidity conditions, respectively. Major changes can be seen in all of these characteristics compared to the initial state. The saturation, water content, and porosity of the samples show different degrees of decline after equilibration under various humidity conditions, and the dry density increases.

The changes in the four characteristics above reflect water loss and shrinkage. This is due to the hydration process experienced by the material in the previous 10.5-year period. The samples were initially in quasi-saturated state, so even a sample equilibrated at RH=98% has been dehydrated. The cause of the dehydration is related to the difference in suction inside and outside the sample. In the process of equilibration under different levels of humidity, since the external suction is greater than the internal suction, moisture in pores is sucked out, causing water loss of the material. Due to different sizes of pores, the suction is different, then, the sample will lose water in larger pores first and then those in smaller pores. As the relative humidity decreases, the initial difference between the internal and external suction increases further, and this behavior becomes more pronounced. The pore will lose more water and shrink further until the internal and external suction forces are equal and the whole sample reaches stable equilibrium. For this reason, as the relative humidity decreases (the suction increases), the water content and porosity of the sample gradually decrease, and the entire sample becomes more compact; that is, the dry density increases. The dehydration shrinkage property is practically controlled by interlayer cations, causing the Na-saturated GBM to loss water and shrink significantly at the aggregate scale (Montes-H *et al*. 2003a). In addition, the particle size and porosity may be also affected by the cation saturation.

3.2 Microstructural characteristics

The distinctive micrographs of the samples after equilibration at different relative humidity are presented in Fig. 4 in order to characterize the greatest possible structural changes. Although the macrostructure was relatively integrated, the micropores and fractures were relatively obvious. The cracks and pores are marked in red, while the widths of typical cracks are marked in green. There are many parameters that reflect void space variation, including maximum pore/fracture size, average pore/fracture size, pore/fracture orientation, etc. (Nagurney *et al*. 2021). Here, considering that it is a two-dimensional case, and in order to visually reflect its variation, the maximum fracture width is marked and the location of the maximum fracture width is determined by the Euclidean distance map. It can be clearly seen that there were various degrees of cracking in the process of shrinkage at different humidity. As can be seen from Fig. 4, more cracks can be observed in specimens equilibrated at low humidity, except for the sample equilibrated at a relative humidity of 85%. From the figure, we can see that the sample equilibrated at RH=85% has the highest degree of crack development considering the maximum width of a single crack. The maximum width of the crack was 19.22 μm, even larger than the maximum value of the sample equilibrated at relative humidity of 11%.

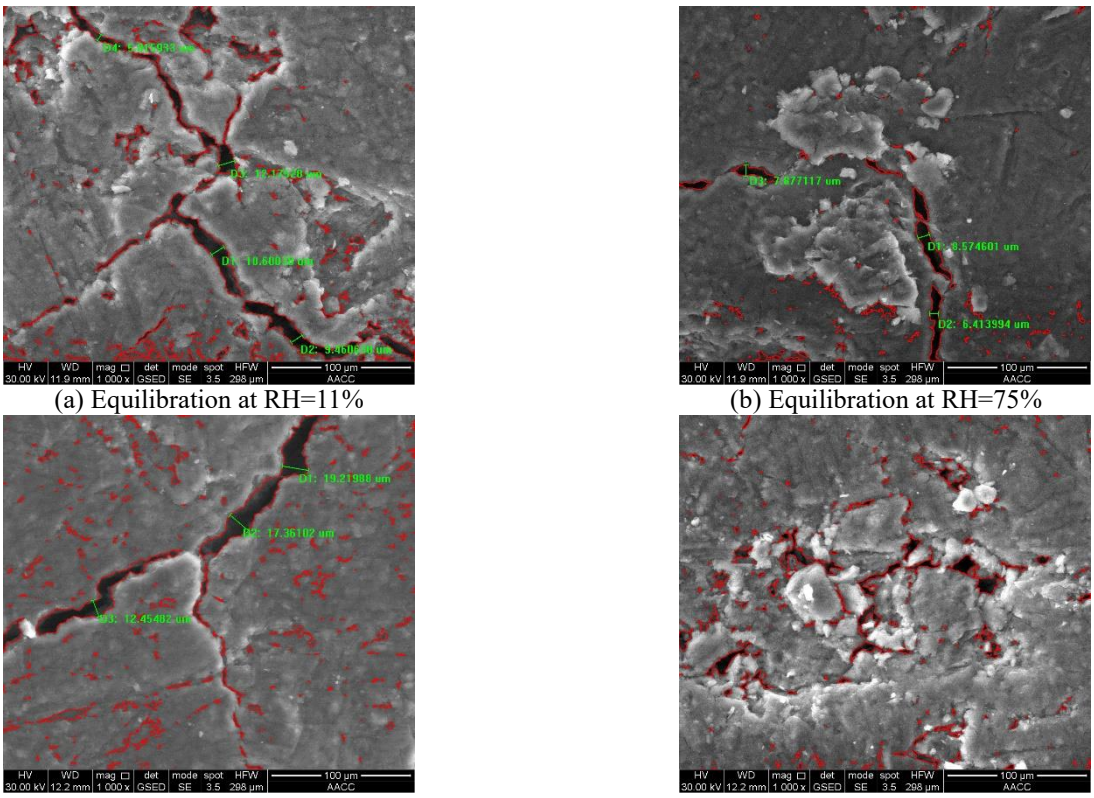

(a) Equilibration at RH=11% (b) Equilibration at RH=75%

(c) Equilibration at RH=85% (d) Equilibration at RH=98%

Fig. 4 Typical microscopic observations of GBM

The GBM samples had been hydrated for many years in the ground before they were extracted, so when they were placed under different relative humidity conditions, they were subjected to a wetting and drying process on the whole.

In general, the dehydration was more significant when the sample equilibrated at lower relative humidity, which caused more cracks to appear (Montes *et al.* 2005). The greater crack opening of the specimen equilibrated at 85% RH mainly attributed to its highest initial dry density. Usually, a sample with a higher dry density is more likely to undergo uneven expansion or shrinkage during water absorption or dehydration, which makes it easier to crack (Saba *et al*. 2014). The crack porosity is closely related to the content of bentonite (Rayhani *et al.* 2007, Tang *et al.* 2008). Due to the excellent capacity to adsorb water and to swell in the previous EB experiment, The GBM has very high initial swelling potentials. When the sample is subjected to shrinkage, it will develop high tensile stress that exceeded the tensile strength of the material, and then lead to the formation and development of cracks (Gebrenegus *et al*. 2011). These cracks may become the main channel for gas flow and then greatly affect permeability.

For small specimens equilibrated at 85% and 98% relative humidity, after ESEM observation, they were dried at 105°C, and then the dried specimens were scanned again by ESEM. Figs. 5(a) and 5(b) shows microphotographs of the samples after 105°C drying. Temperature affected their microstructure greatly. Compared with the balanced structure at different humidity (Figs. 4(c) and 4(d)), the micropores were expanded further and cracks were further formed and developed. Some previously closed cracks expanded further and opened, especially for the one at the relative humidity of 98%. It can be clearly seen that very large cracks formed on the surface. The maximum crack width was 88.46 μm.

Drying practically affects the evaporation of water. The formation of cracks is not necessarily caused by the loss of total water, but the no external water supply to meet the water evaporation demand of the sample surface at high temperature. This will lead to the generation of tensile stress, and then cause the development of cracks. At the same time, due to the early hydration process, the sample equilibration at RH of 98% has higher swelling potentials. This leads to formation of higher tensile stress during the drying process, hence higher development of cracks in the sample at 105℃, as shown in Fig. 5(b). These cracks will become potential dominant channels for seepage. Therefore, it reflects that, in addition to the changes in porosity and water content, the increase of temperature may also cause the formation and development of cracks, which will greatly affect the sealing performance of the whole repository.

3.3 Permeability changes after equilibration under different RH conditions

3.3.1 GBM-1 (RH=11%)

After undergoing the equilibration process in an environment of 11% RH, sample GBM-1 reached a state close to dryness; the water content decreased by a very

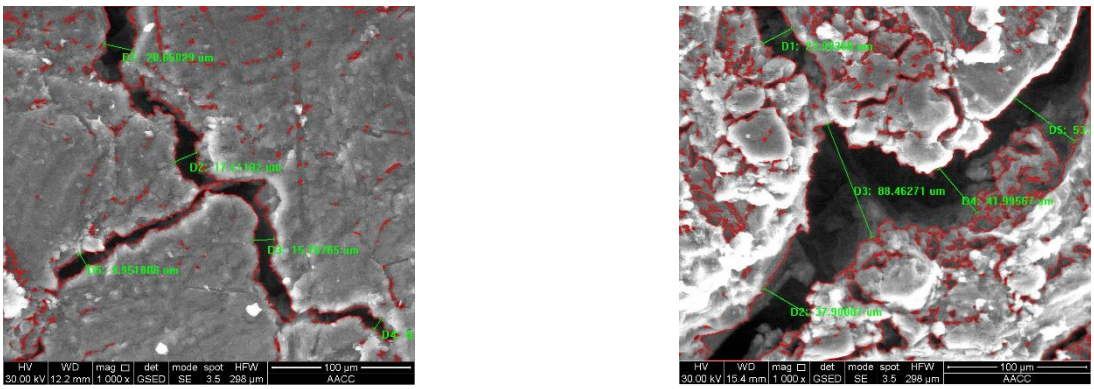

(a) Equilibration at RH=85% (b) Equilibration at RH=98%

Fig. 5 Typical microscopic observations of GBM after 105°C drying

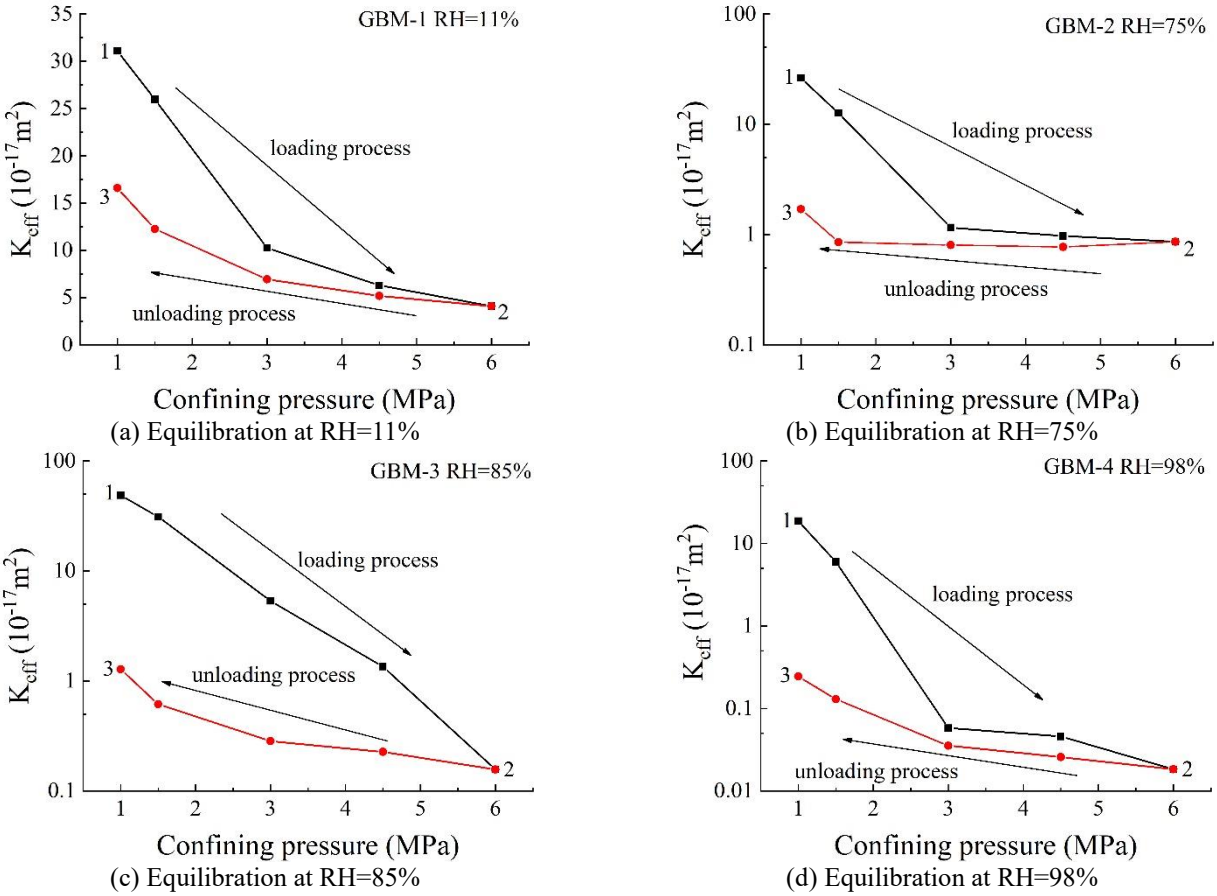

(a) Equilibration at RH=11% (b) Equilibration at RH=75%

(c) Equilibration at RH=85% (d) Equilibration at RH=98%

Fig. 6 Effective gas permeability after equilibration

large degree, reaching 3.24%, and the saturation reached 19.2%. The porosity dropped to 32.50%, indicating pronounced shrinkage of the sample, which also led to a very large increase in the dry density, and the structure of the whole sample became denser.

This macroscopic structural change further affected the gas permeability change in the sample. As shown in Fig. 6(a), when the confining pressure was increased to 6 MPa, the permeability of the sample was only reduced by an order of magnitude. When the confining pressure was brought back down to 1 MPa, the permeability of the sample was restored to the same order of magnitude. The confining pressure had little effect on the permeability of GBM-1 compared with that of the other samples. This can be attributed to the major water-loss shrinkage of sample GBM-1 under this level of humidity; the overall structure was more compact than that of the other samples, and little plastic deformation occurred in the sample during the pressurization process.

3.3.2 GBM-2 (RH=75%)

The permeability change in sample GBM-2 with loading and unloading is shown in Fig. 6(b). This sample experienced a smaller decrease in water content and

saturation than did GBM-1, reaching values of 11.55% and 53.17%, respectively, which are much larger than those of GBM-1. The porosity was also higher than that of GBM-1, at 36.14%, but the dry density was lower (RH=11%), meaning that GBM-2 was less compact than GBM-1.

These differing properties are reflected in the change in permeability. Comparing Figs. 6(a) and 6(b), it can be seen that the permeability of GBM-2 was slightly more sensitive to confining pressure than that of GBM-1. When the confining pressure increased from 1MPa to 6 MPa, the permeability of GBM-2 dropped by two orders of magnitude while that of GBM-1 dropped by one order of magnitude. Moreover, when the sample was unloaded to a confining pressure of 1 MPa, although the permeability was slightly increased, it was still one order of magnitude less than the initial permeability, and the permeability reduction was greater than that of GBM-1. In general, this permeability reduction can be attributed to the higher porosity and water content of GBM-2, which led the sample to have different strength and stiffness properties than GBM-1. Due to its higher degree of saturation, GBM-2 was more easily compressed, making it more sensitive to confining pressure than was GBM-1.

3.3.3 GBM-3 (RH=85%)

As shown in Fig. 3, after equilibration, the water content of sample GBM-3 reached 14.59%, and its saturation reached 63.99%. The dry density was significantly lower than those of the first two samples, at 1.68 g/cm3, and the porosity was 38.35%, which means that the overall structure of the sample was looser than those of the first two samples. The macroscopic structural changes were also reflected in the change in the permeability of the sample with loading and unloading. The influence of confining pressure on permeability was more obvious than for samples GBM-1 and GBM-2. When the confining pressure was increased from 1 MPa to 6 MPa, the permeability was reduced by three orders of magnitude, a much greater drop than that for GBM-1 and GBM-2. When the confining pressure was returned to 1 MPa, the permeability increased to a certain degree but remained lower than the permeability at the initial 1 MPa condition. The two differ by almost two orders of magnitude.

GBM-3 was in a state of higher saturation with more swelling deformation, making it more easily compressed than the first two samples. In addition, as mentioned above, the change in the microstructure can be used to reflect the change in macroscopic permeability. As shown in Fig.4, GBM-3 has the highest degree of crack development in view of the maximum width of a single crack. This is another reason for the highest permeability at the initial moment. And the closure of the largest crack also causes the permeability decrease of GBM-3 at high confining pressure.

The variability of the permeability at 1MPa confining pressure reflects a higher degree of irreversible deformation due to specimen compression than was seen in the first two samples. Relevant studies have shown that shrinkage at higher humidity initially exhibits stronger water loss and shrinkage characteristics (Montes-H *et al.* 2003b). The deformation observed can be attributed to the interaction between the macrostructure and microstructures (particle or aggregate scale, <100 μm) (Lin and Cerato 2014). When a specimen approaching saturation is subjected to pressure, it will show more compression of microstructures and fusion of granular layers.

3.3.4 GBM-4 (RH=98%)

Sample GBM-4 was placed in a higher relative humidity environment (RH=98%) for equilibration. As previously described, because the entire GBM sample was near saturation when not equilibrated, even under such a high humidity, the sample was still in a state of water-loss shrinkage. It can be seen from Fig. 3 that the water content and saturation decreased by 24.71% and 17.99%, respectively, but were still at a much higher level than for the other samples. The porosity of the material decreased by 14.41%, which also led to an increase in its dry density.

The changes in permeability with loading and unloading are shown in Fig. 6(d). Compared with the other samples, the permeability of GBM-4 sample can be seen to have exhibited higher sensitivity at low confining pressure. When the confining pressure rose from 1 MPa to 3 MPa, the permeability decreased by four orders of magnitude. When the confining pressure was increased to 6 MPa, the permeability dropped to 10^{-19} m^2, and the material can be considered to have reached a gas-tight state. When the confining pressure was unloaded to 1 MPa, the permeability was almost three orders of magnitude lower than that when the sample was initially at 1 MPa.

As with sample GBM-3, this is because the higher saturation under such a high humidity means that the sample is initially in a state of major expansion deformation. This is difficult to recover when it is subjected to loading and unloading, which will cause more dramatic changes in its macrostructure than in that of samples at lower saturations. Furthermore, the process of compression will also lead to an increase in saturation during the test, which, in turn, results in lower permeability.

In order to further study the effect of relative humidity on the permeability of GBM, we chose points 1 (loading process, 1 MPa confining pressure), 2 (loading process, 6 MPa confining pressure) and 3 (unloading process, 1 MPa confining pressure) to study the permeability change law. As shown in Fig. 7, when the first 1 MPa of confining pressure was applied, the effective permeability did not increase or decrease with RH, since the saturation and porosity changed simultaneously at different RH values. When the confining pressure rose to 6 MPa, the permeability of each sample dropped markedly. The influence of confining pressure on permeability was dominant at this time, since confining pressure led to a decrease in porosity and an increase in saturation. At the same time, cracks were nearly closed at such a high confining pressure. Fig. 7 shows that the permeability decreased with the relative humidity at 6 MPa, because higher relative humidity caused higher water content or saturation. Although the porosity was greater at higher relative humidity, it was easier compress. When the confining pressure was unloaded to 1 MPa, the permeability of each sample underwent a certain increase, but it was still lower than that when the sample was initially at 1 MPa.

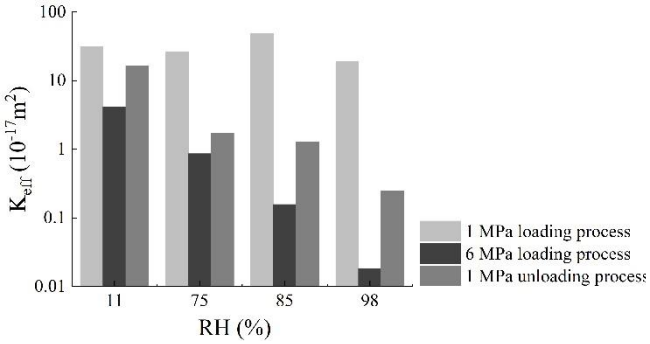

Fig. 7 Effective gas permeability after equilibration at different relative humidities at 1 MPa loading, 1 MPa unloading, and 6 MPa confining pressure

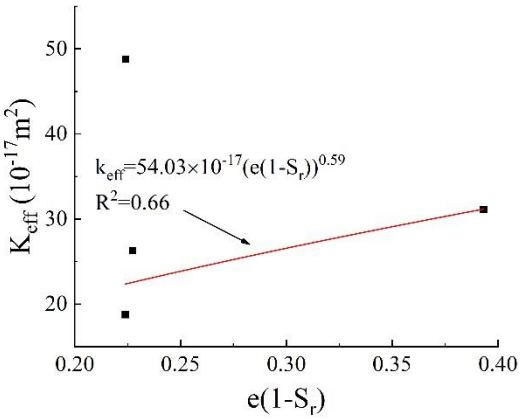

Fig. 8 The relationship between effective gas permeability and the accessible void ratio

In addition, consistent with the situation at 6 MPa, the permeability increased with a decrease in relative humidity, which was completely different from when the sample was initially at 1 MPa. This is due to the large amount of plastic deformation in the loading process. The lower the dry density is, the greater the plastic deformation is, and the easier it is for the sample to maintain its structure after loading. The mechanical effect is dominant, corresponding to a small microstructure change (Cui *et al.* 2013).

Actually, it can be learned from previous research that the gas permeability of bentonite decreases with an increase in dry density and water content and that it is well correlated with the accessible void ratio. The latter expresses the ratio between the gas-accessible volume and the particle volume and is computed as $e(1\text{-}S_r)$ (Carbonell *et al.* 2019, Gutierrez-Rodrigo *et al*. 2014). The effective gas permeability values can then be expressed as follows

$$k_{eff} = a\left(e\left(1-S_r\right)\right)^b \tag{7}$$

where a and b are parameters, e is the void ratio

The Eq. (7) shows that the accessible volume has a higher correlation with the effective gas permeability values than the dry density or water content do. Specifically, the gas permeability increase with the accessible void ratio follows a power law. This is shown in Fig. 8 when four samples under the initial confining pressure of 1 MPa. However, it was quite different for sample GBM-3. In this study, the accessible void ratio of sample GBM-1 is 0.39, while it is 0.22 for sample GBM-3 if we use the porosity and saturation after equilibration for the calculation. It can be clearly seen from Fig. 7 that the effective gas permeability of GBM-3 is higher than the value for GBM-1. The possible reason for this is that GBM-3 has the highest degree of crack development considering the maximum width of cracks, which can be seen from Fig. 4. These cracks were not complete closed under 1 MPa confining pressure, resulting in increased permeability. This also indicates that cracks possibly occurred during the dehydration shrinkage process will become the main channel for gas migration, which will greatly affect its sealing performance.

3.4 Permeability of GBM samples after drying

Samples GBM-3 and GBM-4, which were equilibrated under high humidity (RH=85% and RH=98%), were dried at 105℃ after the gas permeability test had been performed, and the response of the permeability of the dried samples to confining pressure was then determined using the same loading–unloading procedure. The results are shown in Fig. 9. As can be seen from the figure, drying had a major effect on the permeability of the samples, causing an increase in effective gas permeability by 2–3 orders of magnitude compared with its level after equilibration. Moreover, it can be seen that as the confining pressure increases, the permeability gradually decreases, but the extent of the decrease is within one order of magnitude, and the variation is small. In addition, a significant change in gas permeability occurred when the confining pressure rose from 1 MPa to 1.5 MPa, especially for sample GBM-4, which experienced a sudden drop in gas permeability from 1.65×10^{-14} m^2 to 1.96×10^{-15} m^2. Furthermore, it can be seen that even after drying at 105℃, permeability still cannot be restored to the initial state when the confining pressure is reduced from 6 MPa to 1 MPa and that the permeability difference is larger for the sample equilibrated at higher saturation. However, the difference is reduced when comparing it with the permeability before drying (Figs. 6 (c) and 6(d)).

Drying has resulted in the GBM shrinking and becoming more compact, which in turn causes confining pressure to produce only a small change in the volume of pore space. Highly saturated sample develops cracks during the severe shrinkage that occurs during drying, as shown in Fig. 5. Cracks provide preferential pathways for gas flow (Song *et al*. 2018). When the confining pressure rose to 1.5 MPa, the sizes and volume of the cracks reduced, leading to a significant drop in permeability. Other studies have also found the same results that cracks appear on the surfaces of samples as they are dried (Liu *et al.* 2015). The highly saturated sample exhibits higher hysteresis. This is because the wet sample had lower rigidity and strength, making it more easily compressed, and this part of the deformation was mainly plastic, so only a small recovery was possible after pressure was released. When the specimen is dried, its resistance to deformation increases and its plastic deformation decreases under the influence of the confining pressure, which also leads to a smaller difference in permeability compared to that after equilibration in different humidity.

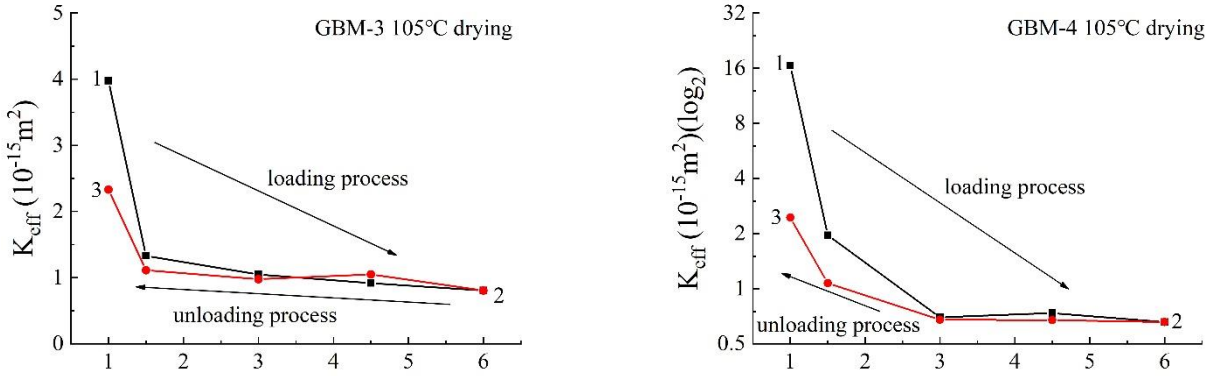

(a) GBM-3, RH=85% (b) GBM-4, RH=98%

Fig. 9 Effective gas permeability after 105°C drying

5. Conclusions

The current study focused on the permeability of unsaturated GBM after 10.5-year groundwater treatment. The effects of relative humidity, confining pressure, and drying were discussed with their changes of microstructural characteristics. The main conclusion are as follows:

- In the water retention test, the samples exhibited dehydration contraction. Samples with higher relative humidity had smaller degrees of water loss, resulting in less shrinkage deformation and making it easier for them to maintain their original state after equilibration.
- In the gas permeability, hysteresis occurred in the change in permeability with confining pressure, and as the relative humidity increased, the degree of hysteresis became larger. It was found that the permeability of samples equilibrated at higher RH to show higher sensitivity to confining pressure and the sample equilibrated under the condition of 98% RH approached the requirement for gas tightness when the confining pressure was increased to 6 MPa.
- The effect of drying on permeability was very obvious. It increased the effective gas permeability of highly saturated samples by 2–3 orders of magnitude and reduced the irreversible change in gas permeability after being subjected to loading and unloading.

In particular, it should be pointed out that in the process of radioactive waste storage, GBM with high degree of hydration can play a sealing role in the early stage. But due to the heat generated by the radioactive waste in the later period, the buffer/backfill material will undergo a process of water loss and shrinkage. A large number of cracks may be generated, which may become the main channel for gas migration, thereby affecting its sealing performance.

Acknowledgments

The research described in this paper was financially supported by the Agence Nationale pour la Gestion des Déchets Radioactifs (ANDRA), the National Natural Science Foundation of China (No. 52174133, 51974296 and U1803118).

References

Angin, Z. and Ikizler, S. B. (2018), "Assessment of swelling pressure of stabilized bentonite", *Geomech. Eng.*, **15**(6), 1219-1225. https://doi.org/10.12989/gae.2018.15.6.1219.

Billiotte, J., Yang, D. and Su, K. (2008), "Experimental study on gas permeability of mudstones", *Phys. Chem. Earth*, Parts A/B/C, **33**, 231-236. https://doi.org/10.1016/j.pce.2008.10.040.

Carbonell, B., Villar, M.V., Martín, P.L. and Gutiérrez-Álvarez, C. (2018), "Gas transport in compacted bentonite after 18 years under barrier conditions", *Geomech. Energ. Environ.*, **17**, 66-74. https://doi.org/10.1016/j.gete.2018.03.001.

Cui, Y.J., Nguyen, X.P., Tang, A.M. and Li, X.L. (2013), "An insight into the unloading/reloading loops on the compression curve of natural stiff clays", *Appl. Clay Sci.*, **83-84**, 343-348. https://doi.org/10.1016/j.clay.2013.08.003.

Cuss, R.J., Harrington, J.F., Noy, D.J., Wikman, A. and Sellin, P. (2011), "Large scale gas injection test (Lasgit): Results from two gas injection tests", *Phys. Chem. Earth*, Parts A/B/C, **36**(17-18), 1729-1742. https://doi.org/10.1016/j.pce.2011.07.022.

Czaikowski, O., Miehe, R. and Rothfuchs, T. (2014), "Self-sealing barriers of sand/clay mixtures – lessons learnt fromin situexperiment and retrospective modelling", Geological Society, London, Special Publications, **400**(1), 381-397. https://doi.org/10.1144/sp400.16.

Dana, E. and Skoczylas, F. (1999), "Gas relative permeability and pore structure of sandstones", *Int. J. Rock Mech. Mining Sci.*, **36**(5), 613-625. https://doi.org/10.1016/s0148-9062(99)00037-6.

Davy, C.A., Skoczylas, F., Lebon, P. and Dubois, T., (2008), "Gas migration properties through a bentonite/argillite interface", *Appl. Clay Sci.*, **42**(3), 639-648. https://doi.org/10.1016/j.clay.2008.05.005.

Dueck, A. (2008), "Laboratory results from hydro-mechanical tests on a water unsaturated bentonite", *Eng. Geology*, **97**(1-2), 15-24. https://doi.org/10.1016/j.enggeo.2007.11.001.

Gallé, C. (2000), "Gas breakthrough pressure in compacted Fo–Ca clay and interfacial gas overpressure in waste disposal context", *Appl. Clay Sci.*, **17**(1-2), 85–97. https://doi.org/10.1016/s0169-1317(00)00007-7.

García-Siñeriz, J., Rey, M. and Mayor, J., (2008), "The engineered barrier experiment at Mont Terri rock laboratory", *Sci. Technol. Series n*, **334**, 65-75, lille, September.

Garcia-Sineriz, J.L., Villar, M.V., Rey, M. and Palacios, B. (2015), "Engineered barrier of bentonite pellets and compacted blocks: State after reaching saturation", *Eng. Geology*, **192**, 33-45. https://doi.org/10.1016/j.enggeo.2015.04.002.

Gatabin, C. (2005), "Selection and THM characterization of the buffer material", Technical Report RT DPC/SCCME 05-704-B. ANDRA.

Gebrenegus, T., Ghezzehei, T.A. and Tuller, M. (2011), "Physicochemical controls on initiation and evolution of desiccation cracks in sand–bentonite mixtures: X-ray CT imaging and stochastic modeling", *J. Contaminant Hydrology*, **126**(1-2), 100-112. https://doi.org/10.1016/j.jconhyd.2011.07.004.

Graham, C.C., Harrington, J.F., Cuss, R.J. and Sellin, P. (2012), "Gas migration experiments in bentonite: implications for numerical modelling", *Mineral. Mag.*, **76**(8), 3279-3292. https://doi.org/10.1180/minmag.2012.076.8.41.

Gutierrez-Rodrigo, V., Villar, M.V., Martin, P.L. and Romero, F.J. (2014), "Gas transport properties of compacted bentonite", *Unsaturated Soils: Research & Applications*, 1-2, 1735-1740. https://doi.org/10.1201/b17034-253.

Harrington, J.F., Graham, C.C., Cuss, R.J. and Norris, S. (2017), "Gas network development in a precompacted bentonite experiment: Evidence of generation and evolution", *Appl. Clay Sci.*, **147**, 80-89. https://doi.org/10.1016/j.clay.2017.07.005.

Lin, B. and Cerato, A.B. (2014), "Applications of SEM and ESEM in Microstructural Investigation of Shale-Weathered Expansive Soils along Swelling-Shrinkage Cycles", *Eng. Geology*, **177**, 66-74. https://doi.org/10.1016/j.enggeo.2014.05.006.

Liu, J.F., Skoczylas, F. and Talandier, J. (2015), "Gas permeability of a compacted bentonite–sand mixture: coupled effects of water content, dry density, and confining pressure", *Can. Geotech. J.*, **52**(8), 1159-1167. https://doi.org/10.1139/cgj-2014-0371.

Liu, J.F., Skoczylas, F., Talandier, J. and Pu, H. (2016), "Dismantling of the EB experiment: Experimental research on the retrieved GBM and bentonite blocks", *Nuclear Eng. Design*, **300**, 297-307. https://doi.org/10.1016/j.nucengdes.2016.01.023.

Liu, J.F., Song, S.B., Liu, J., Huang, B.X., Cao, X.L., Zhang, K. and Skoczylas, F. (2017), "A numerical investigation on the effect of gas pressure on the water saturation of compacted bentonite-sand samples", *Geofluids*, **2017**, 1-12. https://doi.org/10.1155/2017/9010572.

Liu, J., Wu, Y., Cai, C.-Z., Ni, H., Cao, X., Pu, H. and Skoczylas, F. (2018), "Investigation into water retention and gas permeability of Opalinus clay", *Environ. Earth Sci.*, **77**(5), 1-13. https://doi.org/10.1007/s12665-018-7397-3.

Mayor, J.C., García-Siñeriz, J., Alonso, E., Alheid, H. and Blumbling, P. (2005), "Engineered barrier emplacement experiment in Opalinus Clay for the disposal of radioactive waste in underground repositories", Empresa Nacional de Residuos.

Montes-H, G. (2005), "Swelling–shrinkage measurements of bentonite using coupled environmental scanning electron microscopy and digital image analysis", *J. Colloid Interface Sci.*, **284**(1), 271–277. https://doi.org/10.1016/j.jcis.2004.09.025.

Montes-H, G., Duplay, J., Martinez, L., Geraud, Y. and Rousset-Tournier, B. (2003a), "Influence of interlayer cations on the water sorption and swelling–shrinkage of MX80 bentonite", *Appl. Clay Sci.*, **23**(5-6), 309–321. https://doi.org/10.1016/s0169-1317(03)00130-3.

Montes-H, G., Duplay, J., Martinez, L. and Mendoza, C. (2003b), "Swelling-shrinkage kinetics of MX80 bentonite", *Appl. Clay Sci.*, **22**(6), 279-293. https://doi.org/10.1016/S0169-1317(03)00120-0.

Montes-H, G., Geraud, Y., Duplay, J. and Reuschlé, T. (2005), "ESEM observations of compacted bentonite submitted to hydration/dehydration conditions", *Colloids Surfaces A: Physicochem. Eng. Aspects*, **262**(1-3), 14–22. https://doi.org/10.1016/j.colsurfa.2005.03.021.

Nagurney, A.B., Caddick, M.J., Law, R.D., Ross, N.L. and Kruckenberg, S.C. (2021), "Crystallographically controlled void space at grain boundaries in the Harkless quartzite", *J. Struct. Geology*, **143**, 104235. https://doi.org/10.1016/j.jsg.2020.104235.

Niu, W., Ye, W. and Song, X. (2019), "Unsaturated permeability of Gaomiaozi bentonite under partially free-swelling conditions", *Acta Geotechnica*, 1-30. https://doi.org/10.1007/s11440-019-00788-9.

Olivella, S. and Alonso, E.E. (2008), "Gas flow through clay barriers", *Géotechnique*, **58**(3), 157–176. https://doi.org/10.1680/geot.2008.58.3.157.

Ortiz, L., Volckaert, G. and Mallants, D. (2002), "Gas generation and migration in Boom Clay, a potential host rock formation for nuclear waste storage", *Eng. Geology*, **64**(2-3), 287-296. https://doi.org/10.1016/s0013-7952(01)00107-7.

Pusch, R. (1979), "Highly compacted sodium bentonite for isolating rock-deposited radioactive waste products", *Nuclear Technol.*, **45**(2), 153-157. https://doi.org/10.13182/nt79-a32305.

Rayhani, M.H., Yanful, E.K. and Fakher, A. (2007), "Desiccation-induced cracking and its effect on the hydraulic conductivity of clayey soils from Iran", *Can. Geotech. J.*, **44**(3), 276-283. https://doi.org/10.1139/t06-125.

Saba, S., Barnichon, J.D., Cui, Y.J., Tang, A.M. and Delage, P. (2014), "Microstructure and anisotropic swelling behaviour of compacted bentonite/sand mixture", *J. Rock Mech. Geotech. Eng.*, **6**(2), 126-132. https://doi.org/10.1016/j.jrmge.2014.01.006.

Seiphoori, A., Ferrari, A. and Laloui, L. (2014), "Water retention behaviour and microstructural evolution of MX-80 bentonite during wetting and drying cycles", *Géotechnique*, **64**(9), 721-734. https://doi.org/10.1680/geot.14.p.017.

Song, L., Li, J., Garg, A. and Mei, G. (2018), "Experimental study on water exchange between crack and clay matrix", *Geomech. Eng.*, **14**(3), 283-291. https://doi.org/10.12989/gae.2018.14.3.283.

Sun, H. (2018), "A new method to predict swelling pressure of compacted bentonites based on diffuse double layer theory", *Geomech. Eng.*, **16**(1), 71-83. https://doi.org/10.12989/gae.2018.16.1.071.

Sun, H., Mašín, D., Najser, J., Neděla, V. and Navratilova, E. (2018), "Bentonite microstructure and saturation evolution in wetting-drying cycles evaluated using ESEM, MIP and WRC measurements", *Géotechnique*, 1-53. https://doi.org/10.1680/jgeot.17.p.253.

Sun, W., Zong, F., Sun, D., Wei, Z., Schanz, T. and Fatahi, B. (2017), "Swelling prediction of bentonite-sand mixtures in the full range of sand content", *Eng. Geology*, **222**, 146-155. https://doi.org/10.1016/j.enggeo.2017.04.004.

Tang, C.S., Li, S.J., Wang, D.W., Chen, Z.G., Shi, B. and Inyang, H. (2019), "Experimental simulation of boundary condition effects on bentonite swelling in HLW repositories", *Environ. Earth Sci.*, **78**(5), 135. https://doi.org/10.1007/s12665-019-8132-4.

Tang, C., Shi, B., Liu, C., Zhao, L. and Wang, B. (2008), "Influencing factors of geometrical structure of surface shrinkage cracks in clayey soils", *Eng. Geology*, **101**(3-4), 204-217. https://doi.org/10.1016/j.enggeo.2008.05.005.

Villar, M. (2012), "EB experiment. Laboratory infiltration tests report", PEBS Deliverable 2.1-5. Technical Report CIEMAT/2G210/07/12. Madrid.

Wei, T., Hu, D., Zhou, H., Lu, J. and Lü, T. (2019), "Influences of degree of saturation and stress cycle on gas permeability of unsaturated compacted Gaomiaozi bentonite", *Eng. Geology*,

254, 54-62. https://doi.org/10.1016/j.enggeo.2019.04.005.
Xu, L., Ye, W. M. and Ye, B. (2017), "Gas breakthrough in saturated compacted GaoMiaoZi (GMZ) bentonite under rigid boundary conditions", *Can. Geotech. J.*, **54**(8), 1139-1149. https://doi.org/10.1139/cgj-2016-0220.
Zhang, C.L. and Kröhn, K.P. (2019), "Sealing behaviour of crushed claystone-bentonite mixtures", *Geomech. Energ. Environ.*, **17**, 90-105. https://doi.org/10.1016/j.gete.2018.09.004.

CC

Nomenclature

P_1	Gas injection pressure
ΔP	Gas drop pressure
P_0	Atmospheric pressure
Δt	time interval
P_{mean}	Average gas pressure
Q_{mean}	Average flow rate
V_0	Buffer reservoir volume
μ	Dynamic viscosity
k	Permeability
ρ_{bulk}	Bulk density
ρ_d	Dry density
ω	Water content
φ	Porosity
S_r	Saturation
e	Void ratio
a,b	Parameters
Abbreviations	
GBM	Granular Bentonite Material
EB	Engineered Barrier
RH	Relative humidity
FEBEX	Full-Scale Engineered Barriers Experiment
ENRESA	Empresa Nacional de Residuos Radioactivos SA